Construction of variational matrix product states for the Heisenberg spin-1 chain

Jintae Kim [ID],[1] Minsoo Kim [ID],[1] Naoki Kawashima,[2] Jung Hoon Han [ID],[1,*] and Hyun-Yong Lee [ID][3,4,†]

[1]*Department of Physics, Sungkyunkwan University, Suwon 16419, Korea*
[2]*Institute for Solid State Physics, University of Tokyo, Kashiwa, Chiba 277-8581, Japan*
[3]*Department of Applied Physics, Graduate School, Korea University, Sejong 30019, Korea*
[4]*Division of Display and Semiconductor Physics, Korea University, Sejong 30019, Korea*

We propose a simple variational wave function that captures the correct ground-state energy of the spin-1 Heisenberg chain model to within 0.04%. The wave function is written in the matrix product state (MPS) form with the bond dimension $D = 8$ and is characterized by three fugacity parameters. The proposed MPS generalizes the Affleck-Kennedy-Lieb-Tasaki state by dressing it with dimers, trimers, and general q-mers. The fugacity parameters control the number and the average size of the q-mers. Furthermore, the $D = 8$ variational MPS state captures the ground states of the entire family of the bilinear-biquadratic Hamiltonian belonging to the Haldane phase to high accuracy. The 2-4-2 degeneracy structure in the entanglement spectrum of our MPS state is found to match well the results of the density matrix renormalization group (DMRG) calculation, which is computationally much heavier. Spin-spin correlation functions also find an excellent fit with those obtained by DMRG.

I. INTRODUCTION

Examples of exact many-body ground states tied to relatively simple Hamiltonians are extremely rare. A well-known exception is the Affleck-Kennedy-Lieb-Tasaki (AKLT) Hamiltonian [1,2]

$$H_A = \sum_i \left[\frac{1}{3} (\mathbf{S}_i \cdot \mathbf{S}_{i+1})^2 + \mathbf{S}_i \cdot \mathbf{S}_{i+1} + \frac{2}{3} \right], \qquad (1.1)$$

which has a unique ground-state wave function $|A\rangle$ given in simple analytic form. The simplicity of the ground-state wave function is revealed also through its matrix product state (MPS) form, first written down in Refs. [3,4], inspired by the work of AKLT. (See also the general ideas set forth in Refs. [5,6].) The size of the matrix, known as the bond dimension, for the AKLT state is $D = 2$, the smallest dimension allowed in any MPS representation. In the meantime, the ground state of the pure spin-1 Heisenberg model belongs to the same Haldane [7] or the symmetry-protected topological (SPT) [8,9] phase as the AKLT state, and therefore, the two states must in some sense be smoothly connected to each other. One aspect of such adiabatic continuity is the double degeneracy of the entanglement spectrum (ES), which characterizes the whole Haldane (SPT) phase [8].

Although the entanglement aspect of the SPT phase has been confirmed for some time by the numerical density matrix renormalization group (DMRG) method [8], we have not yet seen an active attempt to write down an adiabatic continuation of the AKLT state in analytic form that spans the entire SPT phase. A recent noteworthy effort is Ref. [10], which constructed the family of variational MPS ground states for a spin-1 chain based on a fairly general SU(2) symmetry consideration. Here we present the analytical construction of the family of variational MPS (vMPS) wave functions that spans nearly the entire SPT phase of the so-called bilinear-biquadratic (BLBQ) spin-1 Hamiltonian. Despite the smallness of the bond dimension $D = 8$, our vMPS yields excellent ground-state properties, quite comparable to those obtained by DMRG.

In Sec. II we show how to utilize the perturbative argument to aid one's thinking in constructing proper vMPS wave functions for the BLBQ Hamiltonian. This stands in contrast to the much more formal approach of Ref. [10], which relied heavily upon the symmetry constraint to narrow down the form of the vMPS. In Sec. III some physical properties of our $D = 8$ vMPS are calculated and compared with those obtained by DMRG for the same BLBQ model Hamiltonian. The agreements are quite good for energy and spin-spin correlations and in regard to various entanglement properties. In other words, the problem of finding ground-state wave functions for the SPT phase of the BLBQ Hamiltonian is *practically solved*.

II. CONSTRUCTION OF THE VARIATIONAL MPS WAVE FUNCTION

A. Perturbative approach

A useful way to think about the Heisenberg Hamiltonian H_H is as an AKLT model with perturbation $H_H = H_A + \lambda \sum_i \mathbf{S}_i \cdot \mathbf{S}_{i+1}$, in the limit $\lambda \to \infty$. In this view, modification of the AKLT state occurs by the action of the quadratic

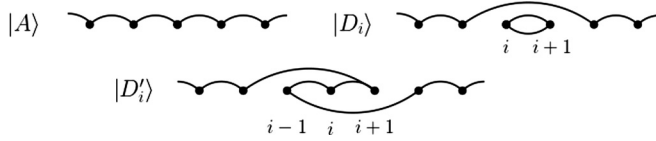*hanjemme@gmail.com
†hyunyong@korea.ac.kr

FIG. 1. Schematic figures for the AKLT state $|A\rangle$, the single-dimer state $|D_i\rangle$, and the extended dimer state $|D_i'\rangle$. Each wavy line connecting the points represents a singlet bond $s^\dagger$ defined in the text.

exchange $\mathbf{S}_i \cdot \mathbf{S}_{i+1}$ on the AKLT state $|A\rangle$. We find

$$\mathbf{S}_i \cdot \mathbf{S}_{i+1}|A\rangle = -|A\rangle + (1/2)|D_i\rangle. \quad (2.1)$$

The new state $|D_i\rangle$, shown in Fig. 1, has a pair of adjacent sites $(i, i+1)$ locked into the total spin-0 *dimer*, while the rest of the sites continue to remain in the AKLT state. In the Schwinger boson (SB) notation for the singlet creation operator $s_{ij}^\dagger = a_i^\dagger b_j^\dagger - b_i^\dagger a_j^\dagger$, we can express the one-dimer state as

$$|D_i\rangle = \left[\left(\prod_{j \neq i-1,i,i+1} s_{j,j+1}^\dagger \right) s_{i-1,i+2}^\dagger \right] (s_{i,i+1}^\dagger)^2 |v\rangle,$$

with $|v\rangle$ being the SB vacuum. The terms inside the square bracket give the AKLT state over the chain with two sites, i and $i+1$, missing. The appearance of an isolated dimer according to Eq. (2.1) was noted by Arovas quite some time ago [11].

According to the first-order consideration above, the ground state of the Heisenberg model differs from the AKLT state by the appearance of a single dimer. At the next order in perturbation we find

$$\mathbf{S}_i \cdot \mathbf{S}_{i+1} |D_i\rangle = -2 |D_i\rangle,$$
$$\mathbf{S}_{i-1} \cdot \mathbf{S}_i |D_i\rangle = |A\rangle + |D_i\rangle + |D_i'\rangle,$$
$$\mathbf{S}_{i+1} \cdot \mathbf{S}_{i+2} |D_i\rangle = |A\rangle + |D_i\rangle + |D_{i+1}'\rangle,$$
$$\mathbf{S}_j \cdot \mathbf{S}_{j+1} |D_i\rangle = -|D_i\rangle + \frac{1}{2} |D_i D_j\rangle, \quad (2.2)$$

where $j \neq i-1, i, i+1$ in the last equation. As one can see, the appearance of the double-dimer configuration $|D_i D_j\rangle$ at the nonoverlapping bonds $(i, i+1)$ and $(j, j+1)$ is the obvious new feature of the second-order perturbation. The other notable feature at second order is the emergence of the configuration denoted $|D'\rangle$, shown graphically in Fig. 1. This new state $|D_i'\rangle$, also discovered by Arovas [11], can be decomposed as the superposition of the AKLT state, one-dimer states $|D\rangle$, and a new, length-2 dimer state defined over the second-nearest neighbors $(i, i+2)$. Seeing how this comes about requires a little bit of preparatory work.

First of all, a simple identity can be proven for the singlet creation operators:

$$s_{ij}^\dagger s_{kl}^\dagger + s_{ik}^\dagger s_{lj}^\dagger + s_{il}^\dagger s_{jk}^\dagger = 0. \quad (2.3)$$

This identity can be used to prove, among others, the following relations:

$$s_{12}^\dagger s_{23}^\dagger s_{34}^\dagger s_{41}^\dagger + s_{13}^\dagger s_{34}^\dagger s_{42}^\dagger s_{21}^\dagger = (s_{12}^\dagger)^2 (s_{34}^\dagger)^2,$$
$$s_{12}^\dagger s_{23}^\dagger s_{34}^\dagger s_{41}^\dagger + s_{13}^\dagger s_{32}^\dagger s_{24}^\dagger s_{41}^\dagger = (s_{14}^\dagger)^2 (s_{23}^\dagger)^2. \quad (2.4)$$
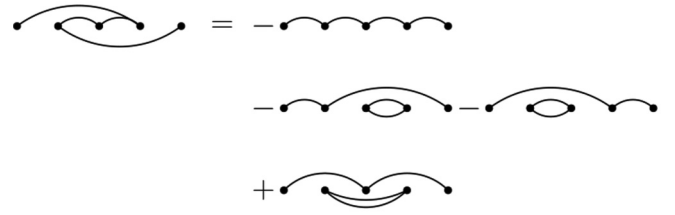

FIG. 2. Graphical proof showing how state $|D'\rangle$ breaks down as the AKLT state and several one-dimer states.

A simple counting argument suggests that there can be three independent ways of producing a *tetramer* (a spin singlet made out of four spin 1's). They are represented in the SB language as $s_{12}^\dagger s_{23}^\dagger s_{34}^\dagger s_{41}^\dagger |v\rangle$, $(s_{12}^\dagger)^2 (s_{34}^\dagger)^2 |v\rangle$, and $(s_{14}^\dagger)^2 (s_{23}^\dagger)^2 |v\rangle$, respectively. All other ways of producing a tetramer, for example, $s_{13}^\dagger s_{34}^\dagger s_{42}^\dagger s_{21}^\dagger |v\rangle$, become their linear combinations according to the identity (2.4).

One can now exploit Eq. (2.4) to prove relations shown graphically in Fig. 2. The $|D'\rangle$ state, as mentioned above, is generated by the second-order action of the exchange Hamiltonian on the AKLT state. Then according to the graphical proof of Fig. 2, the state $|D'\rangle$ breaks down as a linear combination of the AKLT state, some compact one-dimer states, and the long-range one-dimer state shown in the final line of Fig. 2. The main additional feature of the second-order perturbation is therefore the appearance of the long-range dimer.

We examine another aspect of the higher-order perturbation on the AKLT state, starting with the familiar relation

$$(2\mathbf{S}_i \cdot \mathbf{S}_{i+1} + 2)|A\rangle = |D_i\rangle. \quad (2.5)$$

Arranged in this way, it appears that $2\mathbf{S}_i \cdot \mathbf{S}_{i+1} + 2$ is playing the role of the dimer creation operator. In fact this interpretation makes sense once we rewrite the operator in the equivalent form

$$[(\mathbf{S}_i + \mathbf{S}_{i+1})^2 - 2]|A\rangle = |D_i\rangle. \quad (2.6)$$

The AKLT state $|A\rangle$ contains, by construction, only those configurations that have total spin $S = 0$ or $S = 1$ for the $(i, i+1)$ pair of sites. By acting on it with the projection operator $(\mathbf{S}_i + \mathbf{S}_{i+1})^2 - 2$, one ends up eliminating the $S = 1$ component over the $(i, i+1)$ bond. The state that remains after the projection must be the total spin singlet $S = 0$, which we previously called the dimer.

Following a similar line of reasoning, the trimer state (a spin singlet composed of three spin 1's) may be created by the operation

$$[(\mathbf{S}_{i-1} + \mathbf{S}_i + \mathbf{S}_{i+1})^2 - 2][(\mathbf{S}_{i-1} + \mathbf{S}_i + \mathbf{S}_{i+1})^2 - 6]|A\rangle.$$

Out of the three possible total spins $S = 0, 1, 2$ for the $(i-1, i, i+1)$ bond, only the $S = 0$ state will survive after the projection. After expanding, we get

$$(\mathbf{S}_{i-1} \cdot \mathbf{S}_i + \mathbf{S}_i \cdot \mathbf{S}_{i+1} + \mathbf{S}_{i+1} \cdot \mathbf{S}_{i-1})$$
$$\times (\mathbf{S}_{i-1} \cdot \mathbf{S}_i + \mathbf{S}_i \cdot \mathbf{S}_{i+1} + \mathbf{S}_{i+1} \cdot \mathbf{S}_{i-1} + 2)|A\rangle \equiv |T_i\rangle$$

as the trimer state. Hence, it turns out the trimer projection operator also requires the second-order action of the exchange operators on the AKLT state. Gathering all the heuristic
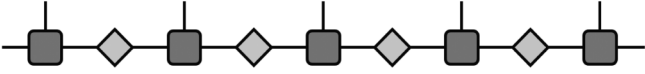
FIG. 3. General graphical representation of the MPS consisting of an alternating site tensor (square with a vertical arm) and bond tensor (diamond, no dangling arm).

arguments thus far, we arrive at a good picture of the kinds of influences that the Heisenberg term exerts on the AKLT state at each order of perturbation.

In the next section, we will apply this sort of perturbative thinking to arrive at a good prescription for the vMPS ground wave function of the Heisenberg model in particular and the BLBQ Hamiltonian in general.

B. Construction of the MPS tensor

The MPS wave function has the general structure of being given by the product of alternating site and bond tensors, as depicted in Fig. 3. We first present the $D = 8$ site tensor in its final form:

$$T = T_1 + T_2 + 4ab^2 T_2^t - 2b T_3 - 3c T_4. \quad (2.7)$$

It consists of four tensors T_1 through T_4 and three mixing parameters a, b, c that are adjusted to lower the energy. The components of the tensors are given out explicitly as

$$[T_1]^s_{ii',jj'} = \left[CG^1_{\frac{1}{2}\frac{1}{2}}\right]^s_{ij}\delta_{i'3}\delta_{j'3},$$

$$[T_2]^s_{ii',jj'} = \left[CG^0_{\frac{1}{2}\frac{1}{2}}\right]^s_{ij}\delta_{i'3}\delta_{j's},$$

$$[T_3]^s_{ii',jj'} = \left[CG^0_{\frac{1}{2}\frac{1}{2}}\right]^s_{ij}\left[CG^1_{11}\right]^s_{i'j'},$$

$$[T_4]^s_{ii',jj'} = \left[CG^1_{\frac{1}{2}\frac{1}{2}}\right]^s_{ij}\left[CG^0_{11}\right]_{i'j'},$$

$$[B]_{ii',jj'} = \left[CG^0_{\frac{1}{2}\frac{1}{2}}\right]_{ij}\left(\left[CG^1_{11}\right]_{i'j'} + \delta_{i'3}\delta_{j'3}\right). \quad (2.8)$$

The bond tensor B (represented by diamonds in Fig. 3) is shown in the last line. T_2^t in Eq. (2.7) is obtained by taking the transpose of the virtual indices, $[T_2^t]^s_{ii',jj'} = [T_2]^s_{jj',ii'}$. Clebsch-Gordon (CG) coefficients $CG^s_{s_1s_2}$ for combining two spins s_1 and s_2 into the spin s are employed above. In the case of CG^0_{11} and CG^1_{11}, the virtual indices i', j' run only over the three possible spin states 0, 1, 2. Nevertheless, we introduce a fourth component, $i', j' = 3$, and make them four-dimensional. This mathematical contraption plays a crucial role in our construction. Meanwhile the unprimed indices are two-dimensional, $i, j = 0, 1$, for a total of $(2 \times 4 = 8)$-dimensional virtual indices, or $D = 8$. The wave function for a given spin basis $|s_1 s_2 \cdots s_N\rangle$ is obtained by taking the tensor product $T^{s_1} B T^{s_2} B \cdots T^{s_N} B$ and contracting the two end indices either with a trace or some boundary vectors.

The product of a site tensor T^s with the adjoining bond tensor B is symbolically written $TB = \overline{T}$. In components,

$$[\overline{T}_1]^s_{ii',jj'} = \left[CG^1_{\frac{1}{2}\frac{1}{2}}\right]^s_{ik}\left[CG^0_{\frac{1}{2}\frac{1}{2}}\right]_{kj}\delta_{i'3}\delta_{j'3},$$

$$[\overline{T}_2]^s_{ii',jj'} = (-\delta_{ij}/2)\delta_{i'3}\left[CG^0_{11}\right]_{sj'},$$

$$[\overline{T}_2^t]^s_{ii',jj'} = (\delta_{ij}/2)\delta_{i's}\delta_{j'3},$$
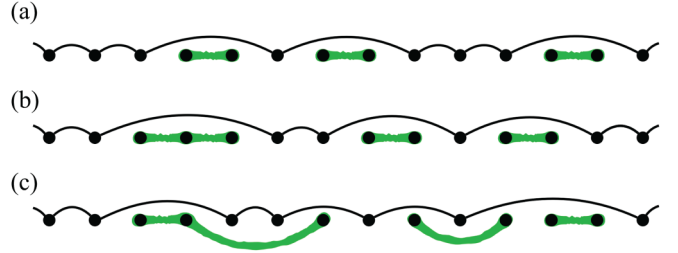

FIG. 4. Exemplary configurations containing (a) multiple compact dimers, (b) two dimers and one trimer (all compact), and (c) long-range q-mers. The black solid line stands for the singlet made out of two $S = 1/2$'s, while the thick green ones are the dimers and trimers.

$$[\overline{T}_3]^s_{ii',jj'} = (-\delta_{ij}/2)\left[CG^1_{11}\right]^s_{i'k'}\left[CG^0_{11}\right]_{k'j'},$$

$$[\overline{T}_4]^s_{ii',jj'} = (\delta_{i'j'}/3)\left[CG^1_{\frac{1}{2}\frac{1}{2}}\right]^s_{ik}\left[CG^0_{\frac{1}{2}\frac{1}{2}}\right]_{kj}. \quad (2.9)$$

The two relations $\left[CG^0_{\frac{1}{2}\frac{1}{2}}\right]_{ik}\left[CG^0_{\frac{1}{2}\frac{1}{2}}\right]_{kj} = -\delta_{ij}/2$ and $\left[CG^0_{11}\right]_{i'k'}$ $\left[CG^0_{11}\right]_{k'j'} = \delta_{i'j'}/3$ were used. Summations over repeated indices are implicit. Note that $\left[CG^1_{\frac{1}{2}\frac{1}{2}}\right]^s_{ik}\left[CG^0_{\frac{1}{2}\frac{1}{2}}\right]_{kj} \equiv A^s_{ij}$ is precisely the MPS tensor that defines the AKLT state. In the simplest case $a = b = c = 0$, the product of T_1 tensors reproduces the AKLT state. The meanings of the full tensors given in Eqs. (2.7) through (2.9) are not easy to grasp at first sight. Below, we explain their meanings by examining specialized cases with only the T_1 and T_2 tensors being nonzero and so on.

To start off, we keep T_1, T_2 and its transpose and examine the resulting MPS state. From the tensor structure shown in Eq. (2.9), one finds that $\overline{T}_2$ can be followed only by $\overline{T}_2^t$ and not by $\overline{T}_1$. This constraint effectively binds $\overline{T}_2$ and its transpose into a pair,

$$[\overline{T}_2]^s_{ii',kk'}[\overline{T}_2^t]^{s'}_{kk',jj'} = (-\delta_{ij}/4)\delta_{i'3}\delta_{j'3}\left[CG^0_{11}\right]_{ss'}.$$

The expression $\left[CG^0_{11}\right]_{ss'}$ is nothing but the wave function of a dimer singlet. The factor $(-1/4)$ in the above combines with the prefactor $4ab^2$ in Eq. (2.7) to give the factor $-ab^2$ to the one-dimer configuration $|D_i\rangle$ depicted in Fig. 1. $\overline{T}_2^t$ can be followed either by $\overline{T}_2$, creating a second dimer in succession to the first, or by $\overline{T}_1$, terminating the dimer and restoring the AKLT chain. The expansion of the tensor product (still omitting T_3 and T_4) gives the series

$$|\psi_{DG}\rangle = \sum_{n=0}^{\infty}\sum_{\Gamma_{DG}^{(n)}}(-a)^n b^{2n}\left|\Gamma_{DG}^{(n)}\right\rangle, \quad (2.10)$$

where the sum n spans the number of dimers and $\Gamma_{DG}^{(n)}$ refers to all possible arrangements of the n dimers ($n = 0$ gives the AKLT state). The two exponents in $(-a)^n b^{2n}$ count the number of dimers n and the total length of the dimers ($2 \times n = 2n$), respectively. For the same fugacities, i.e., the same n, one has all dimer configurations contributing with equal weight to the above sum, a situation we refer to as the dimer gas (DG). An example of the multidimer configuration is shown in Fig. 4(a). The one-dimer configurations in the above sum contribute with a minus sign, $-ab^2$, in accordance

with the prediction of the first-order perturbation. Numerical minimization of the MPS energy indeed proves that $a > 0$ for the variational ground state. Note that all the dimers appearing in the multidimer configuration in Eq. (2.10) are defined over the nearest neighbors; that is, the dimers are "compact."

Next, we restore T_3 but not yet T_4. In addition to the dimer-giving product $\overline{T}_2\overline{T}_2^t$ already discussed, the product $\overline{T}_2(\overline{T}_3)^m\overline{T}_2^t$ with any number of m's is possible. An explicit calculation gives

$$\left[\overline{T}_2\overline{T}_3\overline{T}_2^t\right]_{ii',jj'}^{s_1 s_2 s_3} = (\delta_{ij}\delta_{i'3}\delta_{j'3}/8)$$
$$\times \left[CG_{11}^0\right]_{s_1\alpha}\left[CG_{11}^1\right]_{\alpha\beta}^{s_2}\left[CG_{11}^0\right]_{\beta s_3}. \quad (2.11)$$

The local trimer wave function shown in the second line appears with the weight $-ab^3$, with the exponent 3 representing the presence of a q-mer with $q = 3$. The product $\overline{T}_2(\overline{T}_3)^2\overline{T}_2^t$ generates the local tetramer wave function

$$\left[CG_{11}^0\right]_{s_1\alpha}\left[CG_{11}^1\right]_{\alpha\beta}^{s_2}\left[CG_{11}^0\right]_{\beta\gamma}\left[CG_{11}^1\right]_{\gamma\delta}^{s_3}\left[CG_{11}^0\right]_{\delta s_4}. \quad (2.12)$$

The local q-mer is the trivial representation of the SU(2) spin rotation regardless of its length. One can now read off the general structure of the q-mer wave functions generated by the (T_1, T_2, T_3) construction as

$$|\psi_{QG}\rangle = \sum_{\Gamma_{QG}}(-a)^n b^l\left|\Gamma_{QG}^{(n,l)}\right\rangle. \quad (2.13)$$

The symbol Γ_{QG} refers to any one of the possible mixed q-mer configurations. Configurations with the same total number of q-mers n and their total lengths given by $l = \sum_i q_i n_i$ ($q_i = 2, 3$ for dimers and trimers, respectively) contribute to the wave function with the same weight in this q-mer gas (QG) wave function $|\psi_{QG}\rangle$. An example with one trimer and two dimers ($n = 3$, $l = 7$) is shown in Fig. 4(b). Each q-mer in the expansion is still compact, or defined over q consecutive sites.

As with T_3, the insertion of T_4 can take place only between T_2 and T_2^t. The role of T_4 is to take a compact q-mer and "stretch" it over nonconsecutive sites, without changing the q value. To see this, we include T_1, T_2, T_4 but not T_3 in the site tensor. Possible structures are $\overline{T}_2(\overline{T}_4)^m\overline{T}_2^t$ with arbitrary m. For instance,

$$\left[\overline{T}_1\overline{T}_2\overline{T}_4\overline{T}_2^t\overline{T}_1\right]_{ii',jj'}^{s_1 s_2 s_3 s_4 s_5}$$
$$= -(\delta_{i'3}\delta_{j'3}/12)A_{ik}^{s_1}A_{kl}^{s_3}A_{lj}^{s_5}\left[CG_{11}^0\right]_{s_2 s_4}. \quad (2.14)$$

Indeed, the dimer bond $\left[CG_{11}^0\right]_{s_2 s_4}$ is now over the second neighbors, while the AKLT tensors connect nonadjacent sites 1, 3, and 5. This is precisely the noncompact dimer configuration generated at the second-order perturbation, as mentioned earlier. Expansion of the MPS state (still omitting T_3) gives rise to the long-range dimer gas (LDG),

$$|\psi_{LDG}\rangle = \sum_{\Gamma_{LDG}}(-ab^2)^n(-c)^m\left|\Gamma_{LDG}^{(n,m)}\right\rangle. \quad (2.15)$$

The number m_i of insertions of T_4 in a given dimer gives $m = \sum_i m_i$. It is straightforward now to see that keeping all four

tensors gives the expansion of the variational MPS state:

$$|\psi_{LQG}\rangle = \sum_{\Gamma_{LQG}}(-a)^n b^l(-c)^m\left|\Gamma_{LQG}^{(n,l,m)}\right\rangle. \quad (2.16)$$

Each q-mer has the length $q_i + m_i$. A trimer defined over nonadjacent sites 1, 3, and 5 will contribute $n = 1$, $l = 3$, $m = 2$, for instance, to the weight. This picture of the long-range q-mer gas (LQG) sums up the nature of the variational MPS state we propose in Eqs. (2.7) through (2.9).

The q-mer expansion (2.16) of our vMPS gives a glimpse into the structures of the many-body wave function written in the tensor product form. As one moves away from the exactly solvable AKLT point, the ground state gets dressed by various q-mers of both compact and noncompact natures. The degree to which these q-mers proliferate is governed by the fugacities, of which there are three in our construction. Such intuition is difficult to provide in sheer numerical approaches such as DMRG or in the method adopted in Ref. [10]. It is interesting, to say the least, that the simple-minded perturbative thinking can go a long way in constraining the correct form of the tensor.

In Sec. III we will explore the properties of the $D = 8$ vMPS constructed in this section. Before that, however, it is worth making a critical examination of certain aspects of our vMPS with some mathematical rigor. The following section is devoted to that task.

C. Former aspects of vMPS

Forming a singlet made out of two or three $S = 1$ spins can be done in a unique way; that is, the definitions of the dimer and trimer are unambiguous. On the other hand, there are multiple ways to form the q-mers with $q > 3$. Only one type of q-mer for a given q is generated by our tensor construction, however, and it is important to go over their precise definition. First, we note that the CG tensor $[CG_{11}^1]_{ij}^s$ fuses two $S = 1$ spins into $S = 1$. In order to visualize this process better, we can assign *directions* on the bonds of the CG tensor as follows:

$$[CG_{1,1}^1]_{ij}^s = \quad \quad \quad = - \quad \quad \quad . \quad (2.17)$$

The two inward arrows denote the spins to be fused, while the outward arrow stands for the fused spin. In fact, those directions are related to the so-called quantum number flow [12], particularly the S^z quantum number in our ansatz. That is, the sum of the incoming quantum numbers is identical to the outgoing quantum number. The *empty* arrow in the above diagram is just to reflect the antisymmetric property of the CG tensor, i.e., $[CG_{11}^1]_{ji}^s = -[CG_{11}^1]_{ij}^s$. We should also note the following identity in the quantum number flow:

$$\left[CG_{11}^0\right]_{ik}\left[CG_{11}^1\right]_{kj}^s = \frac{1}{\sqrt{3}}\left[CG_{11}^1\right]_{si}^j,$$

or, identically,

$$= \frac{1}{\sqrt{3}} \times \quad \quad . \quad (2.18)$$

As a result, after multiplying the two CG tensors, the resulting CG tensor fuses a virtual spin i and the physical spin s into another virtual spin, j. As an example, let us consider the five-mer tensor network:

$$(2.19)$$

By absorbing the bond tensor (CG_{11}^0, green diamond in the left diagram) into the site tensor (CG_{11}^1, yellow square in the left diagram), the quantum number flows are changed by virtue of Eq. (2.18), such that the two leftmost (physical) spins are fused into a virtual spin 1, which is then fused with a third physical spin into another virtual spin 1 and so on. In such a way, the physical spin continues to get fused with a virtual spin 1 into another virtual spin 1, until the final virtual spin 1 combines with the final physical spin 1 into the spin singlet. The process is depicted on the right side of Eq. (2.19). This is the precise definition of the q-mer used in this paper.

Our vMPS ansatz preserves the spin rotational symmetry by remaining in a spin singlet state. In other words, the state transforms trivially under an arbitrary global spin rotation $\mathcal{R}(\theta) = \bigotimes_i R_i(\theta)$, with $R_i(\theta) = e^{i\theta\hat{n}\cdot\vec{S}_i}$ and an arbitrary unit vector $\hat{n}$, i.e., $\mathcal{R}|\psi\rangle = e^{i\phi}|\psi\rangle$. The AKLT state is already a spin singlet, and it remains to prove that various q-mers are also singlets. In what follows, we show how the structure of the bond tensor guarantees the spin singlet nature of the q-mers. To this end, we first notice the following two mathematical relations:

$$R(\theta)_{ik} R(\theta)_{jk'} \left[CG_{11}^0\right]_{kk'} = \left[CG_{11}^0\right]_{ij},$$

$$R(\theta)_{ss'} \left[CG_{11}^1\right]_{ij}^{s'} = R(\theta)_{ki} R(\theta)_{k'j} \left[CG_{11}^1\right]_{kk'}^s, \quad (2.20)$$

or, diagrammatically,

Interpretation of the first identity is as follows. One may well consider the CG matrix as a vector by combining the two indices $[CG_{11}^0]_{ij} \to [CG_{11}^0]_{(ij)}$, and then this new CG vector can be regarded as a wave function representing the singlet state of the two $S = 1$ spins. Consequently, it transforms trivially under $R(\theta)$. For the second identity, we can interpret the left side of the equation as the R matrix rotating the physical spin s', which was in turn made by fusing two virtual spins (i, j). On the other hand, two virtual spins (k, k') are rotated before being fused into the physical s on the right side of the equality. Therefore, the second identity implies that the rotation of the physical spin after the fusion of two virtual spins is identical in its effect on the rotation of two virtual spins before the fusion takes place. Using these two identities, one can prove that the arbitrary q-mer is a spin singlet.

As an example, the tetramer wave function under the spin rotation is shown diagrammatically as

$$(2.21)$$

The second relation in Eq. (2.20) is used for the equality of the first and second diagrams, and the first relation is used for the second diagrammatic identity above. It clearly shows that $\mathcal{R}(\theta)|\text{tetramer}\rangle = |\text{tetramer}\rangle$ regardless of θ. The argument easily generalizes to arbitrary q-mer states.

III. GROUND-STATE PROPERTIES

A. Heisenberg model

To test the validity of $|\psi_{\text{LQG}}\rangle$ as a good variational ground state of the Heisenberg model, first, we calculate the average of the nearest-neighbor spin interaction

$$E(a, b, c) = \langle\psi_{\text{LQG}}|\mathbf{S}_i \cdot \mathbf{S}_{i+1}|\psi_{\text{LQG}}\rangle. \quad (3.1)$$

To warm up, we first include only the (T_1, T_2) tensors and vary the coefficient $4ab^2$ in Eq. (2.7) to find that this simple ansatz already gives $E_{\text{DG}} = -1.3920$, in good comparison to the value found by DMRG [13], which is $E_{\text{DMRG}} = -1.4015$. This is a clear improvement over the energy of the AKLT state $E = -4/3 = -1.3333$. Energy improves progressively with the inclusion of more tensors, $E_{\text{LDG}} = -1.3991$ and $E_{\text{QG}} = -1.3998$, until $E_{\text{LQG}} = -1.40097$ at $(a, b, c) = (6.8990, 0.2116, 0.3564)$ becomes only 0.04% higher than E_{DMRG} despite the small bond dimension $D = 8$. It is remarkable that such a simple three-parameter optimization can produce an energy that is comparable to DMRG and modern tensor network algorithms [14,15], which is typically done by optimizing about $D^2 \sim 10^4$–10^6 parameters.

The spin-spin correlation function of the LQG state, shown in Fig. 5(a), is in good agreement with the DMRG results with $\langle\mathbf{S}_0 \cdot \mathbf{S}_n\rangle_{\text{LQG}}/\langle\mathbf{S}_0 \cdot \mathbf{S}_n\rangle_{\text{DMRG}} = 0.9996, 0.9948, 0.9852, 0.9541, 0.9085$ for $n = 1, 2, 3, 4, 5$, respectively. Meanwhile, there is a significant change in the estimated correlation length ξ, which grows as $\xi_{\text{DG}} < \xi_{\text{QG}} < \xi_{\text{LDG}} < \xi_{\text{LQG}} < \xi_{\text{DMRG}}$, as specified in the caption of Fig. 5. The entanglement spectrum shown in Fig. 5(b) displays the 2-4-2 degeneracy regardless of the (a, b, c) parameters chosen, except at $a = 0$ (AKLT state), where only a single pair of degenerate levels appears. The double degeneracy is the characteristic of the SPT phase protected by the $\mathbb{Z}_2 \times \mathbb{Z}_2$ spin rotation symmetry [8]. In fact, the virtual legs in our $D = 8$ tensor accommodate the spin representation $\frac{1}{2} \otimes (0 \oplus 1)$, which is identical to $\frac{1}{2} \oplus \frac{3}{2} \oplus \frac{1}{2}$, leading to the 2-4-2 degeneracy. Furthermore, the two
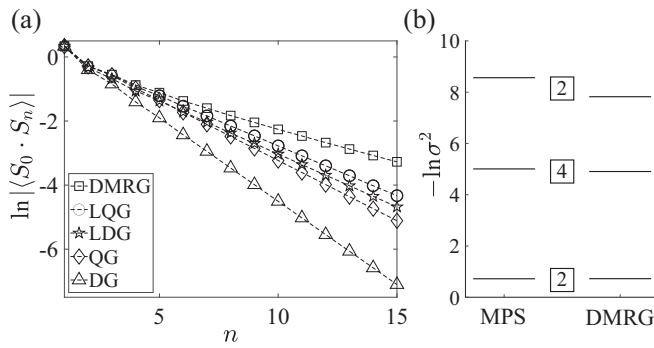
FIG. 5. (a) Spin-spin correlation function $\ln(|\langle \mathbf{S}_i \cdot \mathbf{S}_{i+n} \rangle|)$ [omitting the oscillatory factor $(-1)^n$] obtained from the four variational MPS states: DG, QG, LDG, and LQG. DMRG results are shown for comparison. Corresponding inverse slopes, also called correlation lengths, are 5.0940 (DMRG), 3.2143 (LQG), 3.0299 (LDG), 2.6580 (QG), and 1.9249 (DG) by fitting the large-n parts of the data with the linear function. (A larger correlation length of 6.03 was obtained in Ref. [13] using a different fitting procedure.) (b) Entanglement spectrum obtained from the LQG state and DMRG. The degeneracy of each level is indicated beside the levels. All variational calculations are performed to optimize the Heisenberg exchange energy, Eq. (3.1).

lowest-lying entanglement spectra from the LQG state compare favorably with those of DMRG and modern state-of-the-art algorithms [14,15]: $-\ln \sigma^2 = 0.7207, 5.0060, 8.5652$ for MPS and $0.7242, 4.9045, 7.8227$ for DMRG [16].

B. BLBQ model

The Heisenberg and the AKLT models are two special examples of the BLBQ spin Hamiltonian [17],

$$H(\theta) = \sum_i [\cos \theta (\mathbf{S}_i \cdot \mathbf{S}_{i+1}) + \sin \theta (\mathbf{S}_i \cdot \mathbf{S}_{i+1})^2], \quad (3.2)$$

with $\theta = 0$ and $\theta_A = \tan^{-1}(1/3)$ corresponding to the Heisenberg and AKLT points, respectively. We performed optimization of the LQG for $0 \leqslant \theta \leqslant \theta_A$, with various results shown in Fig. 6. The variational energy of the LQG [Fig. 6 (a)] remains in excellent agreement with the DMRG for the whole range of θ. In addition, the entanglement spectrum and entropy are captured well all over the phase diagram, as shown in Figs. 6 (b) and 6 (c), respectively. The weight a, mainly responsible for the average number of dimers in the ground state, increases linearly with θ, as shown in Fig. 6(d). The other parameters b and c, having to do with the control over the average size q and the spatial extent of the q-mer, remain nearly constant throughout the phase diagram.

Now we let θ vary over the entire Haldane (SPT) phase $-\pi/4 < \theta < \pi/4$ of the BLBQ Hamiltonian. Figure 7 shows the energy of the optimized MPS state (LQG state) at various θ values of the BLBQ Hamiltonian. The DMRG values for the energy are also plotted for comparison. Two different kinds of runs were done for DMRG, the one where the maximum bond dimension D was fixed to 8 (the same as our variational MPS) and one where a much bigger maximum bond dimension was used. The energy difference between our vMPS and the DMRG typically occurs in the third significant digit, except when θ is close to either of the critical points $\theta = \pm \pi/4$. The
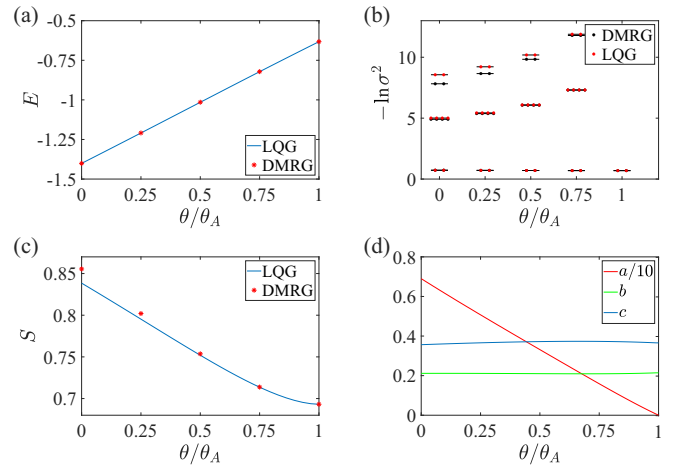

FIG. 6. Variational MPS optimization for the BLBQ model $H(\theta)$. (a) Variational energy vs θ. Lines are from $D = 8$ variational MPS after optimization, and squares are from the DMRG. Differences in energy occur in the fourth significant digits. (b) Entanglement spectrum vs θ. The two lowest sets of levels agree very well between variational MPS and DMRG. (c) Entanglement entropy vs θ. (d) Optimized (a, b, c) vs θ. The a values have been scaled down by a factor of 10 for clarity.

DMRG energy was evaluated by taking the average of the local Hamiltonian $H_i = \cos \theta (\mathbf{S}_i \cdot \mathbf{S}_{i+1}) + \sin \theta (\mathbf{S}_i \cdot \mathbf{S}_{i+1})^2$ for i at the middle of the open chain. The chain size employed in the DMRG was 3×10^3. No size dependence in the energy is discernible at this lattice size.

Finally, Fig. 8 shows the spin-spin correlation functions obtained by optimized MPS (LQG) and by DMRG at several θ values of the BLBQ model. Again, one finds very good agreement, leaving little doubt that our $D = 8$ vMPS captures various aspects of the ground-state wave function with very high accuracy for the whole Haldane phase of the BLBQ model.

IV. DISCUSSION

All in all, the variational MPS state with a small bond dimension $D = 8$ does a good job expressing the ground states of the Haldane phase. Employing a variational MPS state with an even larger bond dimension will improve the
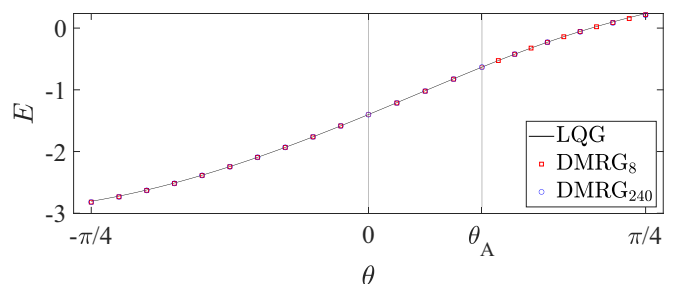

FIG. 7. Energy per site obtained by optimized MPS (LQG) and DMRG. Two different DMRG runs were done and are indicated by the subscript DMRG$_D$ with the maximum bond dimension D used in the calculation.
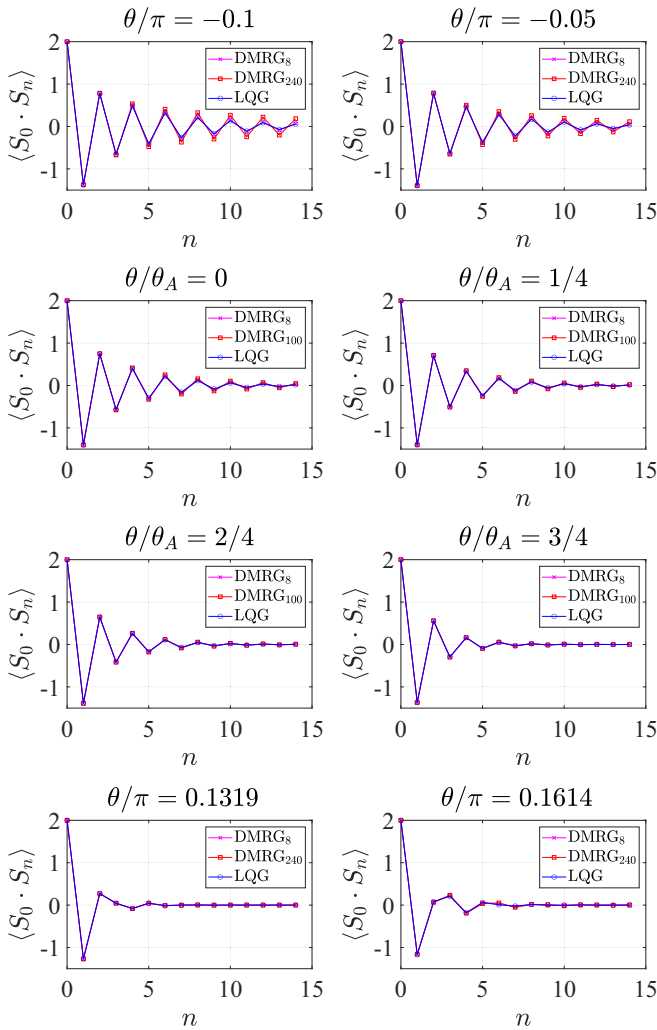
FIG. 8. The spin-spin correlation functions obtained by optimized MPS and DMRG.

an approach. Note that even the DMRG calculation with the restricted $D = 8$ bond dimension yields better energetics than the three-parameter vMPS we have proposed, meaning that further fine tuning with even more variational parameters is possible within the $D = 8$ space for minute improvement in energetics.

It is worth summarizing the advantages of the analytic vMPS form that we propose. Besides the ability to capture good energetics with a simple tensor form and a small number of variational parameters, our vMPS can help us understand the robust 2-4-2 degeneracy structure of the entanglement spectrum through the Haldane phase. Any attempt to capture the ES structure correctly will have to involve a bond dimension no less than $8 (= 2 + 4 + 2)$, and in that regard our vMPS provides a sort of *minimal wave function* for which the 2-4-2 structure can possibly be reproduced.

Second, as the careful argument in Sec. II suggests, there is a certain connection between the usual perturbative way to find corrections to the zeroth-order wave function, i.e., the AKLT state in our case, and what such perturbations imply for the MPS-type wave function. We find that such hybrid thinking (perturbation + MPS) can lead to fruitful results.

For sure, no clever choice of the vMPS wave function can defeat the DMRG in terms of sheer energetics. On the other hand, the wave function finally produced by the DMRG machinery will be incapable of providing the kind of intuitive picture of the ground state, which the vMPS may easily do. In the case of the BLBQ family of Hamiltonians, the physical picture of the ground state over the whole Haldane phase $-\pi/4 < \theta < \pi/4$ is that of the AKLT *parent state*, dressed by proliferation of various dimers, trimers, and so on. The number and extent of the q-mers are controlled by a handful of fugacity parameters, as the expansion (2.16) clearly indicates. This is a valuable insight provided by the analytic vMPS construction.

accuracy of the entanglement entropy and the correlation length compared to the DMRG, at the expense of employing further variational parameters. Indeed, a theory of formal expansion of MPS tensors in terms of irreducible representation of SU(2) was developed and applied to the spin-1 BLBQ model before [10] and found energies that are better than what our $D = 8$ vMPS can predict. In a way this is expected, as dozens of optimization parameters could be employed in such

[1] I. Affleck, T. Kennedy, E. H. Lieb, and H. Tasaki, Phys. Rev. Lett. **59**, 799 (1987).

[2] I. Affleck, T. Kennedy, E. H. Lieb, and H. Tasaki, Commun. Math. Phys. **115**, 477 (1988).

[3] A. Klumper, A. Schadschneider, and J. Zittartz, J. Phys. A **24**, L955 (1991).

[4] A. Klümper, A. Schadschneider, and J. Zittartz, Z. Phys. B **87**, 281 (1992).

[5] M. Fannes, B. Nachtergaele, and R. F. Werner, Europhys. Lett. **10**, 633 (1989).

[6] M. Fannes, B. Nachtergaele, and R. F. Werner, Commun. Math. Phys. **144**, 443 (1992).

[7] F. D. M. Haldane, Phys. Rev. Lett. **50**, 1153 (1983).

[8] F. Pollmann, A. M. Turner, E. Berg, and M. Oshikawa, Phys. Rev. B **81**, 064439 (2010).

[9] X. Chen, Z.-C. Gu, Z.-X. Liu, and X.-G. Wen, Phys. Rev. B **87**, 155114 (2013).

[10] R. Zadourian, A. Fledderjohann, and A. Klümper, J. Stat. Mech. (2016) 083101.

[11] D. P. Arovas, Phys. Lett. A **137**, 431 (1989).

[12] U. Schollwöck, Ann. Phys. (NY) **326**, 96 (2011).

[13] S. R. White and D. A. Huse, Phys. Rev. B **48**, 3844 (1993).

[14] J. Haegeman, J. I. Cirac, T. J. Osborne, I. Pizorn, H. Verschelde, and F. Verstraete, Phys. Rev. Lett. **107**, 070601 (2011).

[15] V. Zauner-Stauber, L. Vanderstraeten, M. T. Fishman, F. Verstraete, and J. Haegeman, Phys. Rev. B **97**, 045145 (2018).

[16] ITensor Library, version 3.1.1, http://itensor.org.

[17] O. Legeza, J. Sólyom, L. Tincani, and R. M. Noack, Phys. Rev. Lett. **99**, 087203 (2007).